Journal of Innovative Optical Health Sciences
Vol. 3, No. 3 (2010) 203–211

DOI: 10.1142/S179354581000099X

PARAMETRIC STUDY OF TISSUE OPTICAL CLEARING BY LOCALIZED MECHANICAL COMPRESSION USING COMBINED FINITE ELEMENT AND MONTE CARLO SIMULATION

WILLIAM C. VOGT, HAIOU SHEN and GE WANG
School of Biomedical Engineering and Sciences
Virginia Polytechnic Institute and State University
ICTAS Bldg., Stanger St., Blacksburg
Virginia 24061, USA

CHRISTOPHER G. RYLANDER
School of Biomedical Engineering and Sciences
Department of Mechanical Engineering
ICTAS Bldg., Virginia Polytechnic Institute and State University
Blacksburg, Virginia 24061, USA
cgr@vt.edu

Tissue Optical Clearing Devices (TOCDs) have been shown to increase light transmission through mechanically compressed regions of naturally turbid biological tissues. We hypothesize that zones of high compressive strain induced by TOCD pins produce localized water displacement and reversible changes in tissue optical properties. In this paper, we demonstrate a novel combined mechanical finite element model and optical Monte Carlo model which simulates TOCD pin compression of an *ex vivo* porcine skin sample and modified spatial photon fluence distributions within the tissue. Results of this simulation qualitatively suggest that light transmission through the skin can be significantly affected by changes in compressed tissue geometry as well as concurrent changes in tissue optical properties. The development of a comprehensive multi-domain model of TOCD application to tissues such as skin could ultimately be used as a framework for optimizing future design of TOCDs.

Keywords: Finite element; Monte Carlo; optical clearing; porcine skin; tissue compression.

1. Introduction

Skin is a complex medium composed of several constituents, including water, collagen, lipids, and various types of cells. All of these materials have different optical properties, creating a mismatch in refractive index and resulting in a highly turbid medium.[1] This scattering significantly decreases the light penetration depth through the tissue and limits the effectiveness of light-based diagnostic applications (e.g., Optical Coherence Tomography) as well as therapeutic treatments (e.g., photodynamic therapy). "Tissue optical clearing" can mitigate the scattering in tissues in order to improve efficacy of these light-based diagnostic and therapeutic therapies. Much work in optical clearing has focused on administration of various chemical agents to increase efficacy of such treatments.[2–10] Tissue dehydration has been shown to be another

potential mechanism of optical clearing, where lower tissue water content results in greater refractive index matching between tissue constituents, thus reducing scattering.[11–14] Previous work has demonstrated that localized mechanical compression can induce an optical clearing effect in porcine skin.[15,16] This clearing effect is thought to be the result of reversible lateral water displacement within the tissue, reducing local refractive index mismatch in compressed tissue regions and changing absorption and scattering behavior. Tissue Optical Clearing Devices (TOCDs) consist of an array of pins within a chamber. Light may be delivered through these pins for either diagnostic or therapeutic applications. Vacuum pressure is applied to stretch the tissue between the pins, creating a reaction force that compresses the tissue beneath the pins, increasing light transmission. Figure 1 shows a prototypical TOCD fabricated using stereolithography. Other TOCDs capable of delivering light through an array of pins are described elsewhere.[15,16]

We suspect that compressive tissue strain during application of the TOCD will result in interstitial water transport and modified tissue optical properties. In this work we present a novel combination of mechanical finite element modeling and optical Monte Carlo simulation that provides insight from a modeling perspective into the effects of altering optical properties within a subregion of a turbid medium undergoing localized compression. The development of a comprehensive multi-domain model of mechanical tissue optical clearing will provide a basis for optimizing the design of future TOCDs.

Fig. 1. Prototypical TOCD made using stereolithography. A 10 mm × 17 mm chamber is filled with an array of pins. A tube is connected to the chamber to apply vacuum pressure when a seal is formed while in contact with the tissue surface.

2. Modeling Methods

2.1. *Mechanical finite element model*

In order to simulate TOCD application to tissue, a simple two-dimensional finite element model of skin compression by a single pin was developed using Abaqus (SIMULIA Inc., Providence, USA) as shown in Fig. 2. A simulated 8 mm × 8 mm × 2.5 mm slab of *ex vivo* porcine skin is placed between an 8 mm × 8 mm × 1 mm glass slide and a 3-mm-diameter hemispherical glass pin. The skin was modeled as a deformable solid, and the glass slide and pin were modeled as analytical rigid bodies since glass will undergo negligible deformation relative to the deformation of the skin sample. The pin is constrained during simulation such that it will translate downward into the skin by 0, 0.625, or 1.5 mm, corresponding to 0, 25, and 50% nominal tissue compressive strain, respectively.

Porcine skin was modeled as a nearly-incompressible hyperelastic material. The mechanical material law for porcine skin was defined using a

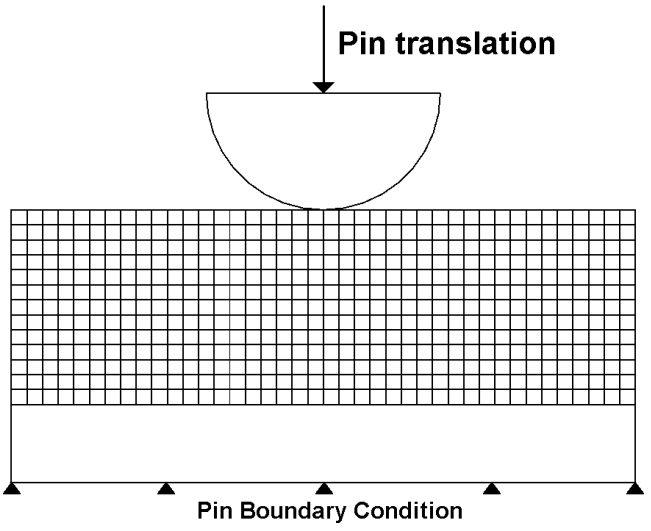

Fig. 2. Sketch of finite element model of local pin compression, showing the deformable skin sample between a rigid slide and pin.

nominal stress/strain curve acquired from local pin compression experiments described previously.[17] In these experiments, a BOSE Electroforce® mechanical tester was used to collect local pin compression load/displacement data. Nominal stress was calculated using the diameter of the pin, while nominal strain was calculated from crosshead displacement. This stress/strain curve was then used to fit a strain energy potential function, U, to the data using nonlinear regression within Abaqus. The Ogden form for U was selected for its robust ability to fit data at higher strains. Regression using other forms of strain energy potential functions, including Neo–Hookean, Yeoh, and Mooney–Rivlin forms was performed but showed that the Ogden form gave the best fit. In Abaqus, the Ogden model is written as

$$U = \sum_{i=1}^{N} \frac{2\mu_i}{\alpha_i^2}\left[\left(\frac{\lambda_1}{J^{\frac{1}{3}}}\right)^{\alpha_i} + \left(\frac{\lambda_2}{J^{\frac{1}{3}}}\right)^{\alpha_i} + \left(\frac{\lambda_3}{J^{\frac{1}{3}}}\right)^{\alpha_i} - 3\right] + \sum_{i=1}^{N} \frac{1}{D_i}(J-1)^{2i}, \quad (1)$$

where N, μ_i, α_i, and D_i are fitting parameters, λ_{1-3} are the orthogonal stretch ratios, and J is the total volume change. By assuming near-incompressibility, the Poisson's ratio, υ, for skin, which is used to fit D_i, was chosen to be equal to 0.49, where $\upsilon = 0.5$ corresponds to complete incompressibility. Based on the fitted curves for Ogden models with different values of N, $N = 3$ yielded the best fit material law that was stable for all strains, as shown in Fig. 3. The resulting parameter values are provided in Table 1. Using these material properties, the finite element simulation was performed in Abaqus, assigning a mesh of 8000 quadrilateral (CPS4R) elements to the deformable skin block. The bottom of the glass slide was assumed to be rigidly pinned, and the bottom of the skin sample was assumed to remain in contact with the glass slide. The validity of this condition depends on the skin sample size relative to the pin diameter. For smaller samples, the edges of the sample may be lifted due to the central compression generating an effective moment to raise the outer edges of the skin. However, this effect would be minimal in a larger skin sample due to the weight of the outer tissue preventing rising of the sample. *In vivo* skin could also be considered semi-infinite relative to the pin size. *In vivo* skin is connected to a layer of fat that binds it to a lower surface, which justifies the constant contact constraint. We chose to use a relatively small skin sample but to also include boundary conditions that essentially define a semi-infinite tissue sample. A smaller skin sample results in lower computational time during optical Monte Carlo simulation since fewer elements will be required for a given average tetrahedral element size.

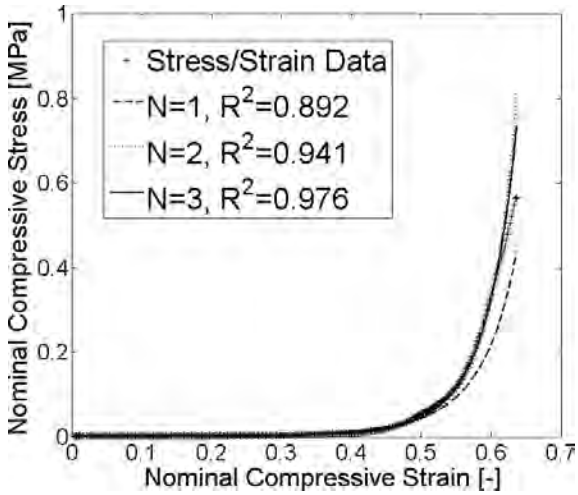

(a)

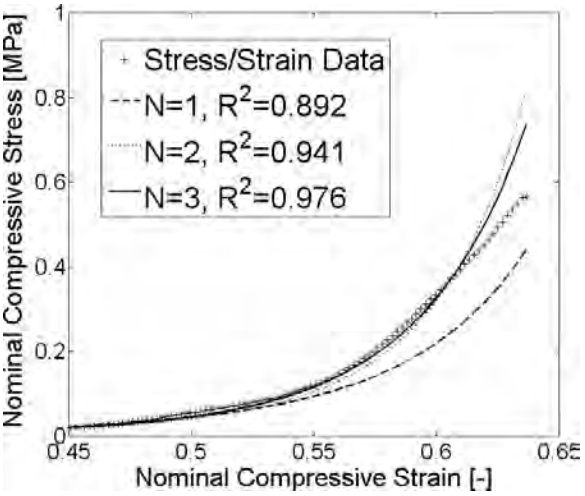

(b)

Fig. 3. Fitted Ogden hyperelastic material models. Strain is plotted starting at (a) 0.0, and (b) 0.45 in order to show detail at higher strains.

Table 1. Fitted Ogden parameters used for hyperelastic material law for skin.

i	μ_i [MPa]	α_i[–]	D_i [MPa^{-1}]
1	−0.24098	−4.3681	18.80
2	0.11934	−3.9035	0.0
3	0.12379	−4.7275	0.0

Assuming that lateral water transport is the mechanism behind mechanical optical clearing, then regions of high strain will have different optical properties relative to unstrained regions. This inhomogeneous distribution of optical properties in a complex geometry motivates the use of optical Monte Carlo modeling to accurately predict modified spatial fluence and light transmission through this medium.

2.2. *Optical Monte Carlo simulation*

Photon propagation can be accurately described by the radiation transfer equation (RTE).[18,19] While the RTE equation is highly complex, approximation methods were developed to solve the RTE, for example the diffusion approximation (DA).[20] Based on our best knowledge, most of the current approximation solvers cannot deal with internal regions with different refractive indices. Monte Carlo simulation is an alternative method to solving the RTE equation that simulates potential photon paths through a medium for many photons. In order to achieve high enough accuracy, Monte Carlo simulations need to simulate enough photons and traditionally required large computation times for complex geometry. Recently, we developed a highly efficient optical Monte Carlo solver called "Tetrahedron-based Inhomogeneous Monte Carlo Optical Simulator" (TIM-OS), which can deal with highly complex geometry.[21]

The geometry of our problem is particularly challenging, as shown in Fig. 1. The photons leaving portions of the pin that were not in direct contact with the skin may still enter into the skin through the air gap between the pin surface and the skin that is not in direct contact with the pin. Since TIM-OS assumes that a photon will be terminated if it escapes from the boundary of the medium, it cannot simulate photons that first escaped from the boundary and then came back into another part of the medium. In order to ensure photons are not lost from the outer edges of the pin, we not only model the pin and the tissue in the medium, but also include a region of air, as shown in Fig. 4, to create a meshed region allowing photons to exit the pin, traverse the air gap, and enter the tissue.

While most mechanical finite element simulations are comprised of several bodies meshed independently of each other, an optical Monte Carlo simulation requires a single contiguous mesh such

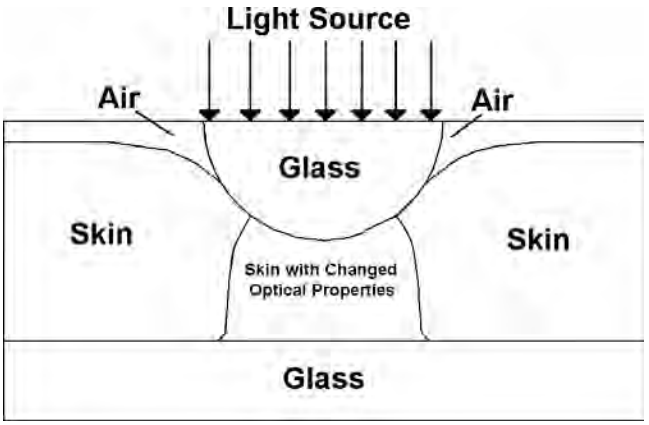

Fig. 4. Composite geometry used in optical Monte Carlo simulation for 50% nominal tissue strain. The arrows represent the defined light source impinging on the upper pin surface.

that all surfaces share common nodes and element faces in order to properly define photon transmission through each element. Also, whereas the mechanical simulations in Abaqus were performed in two dimensions to reduce computation time, TIM-OS uses a three-dimensional framework to reliably predict light scattering. A three-dimensional model was constructed as shown in Fig. 4. This inhomogeneous medium was chosen to be comprised of four regions: the glass pin and slide, the air between the pin and skin surfaces, the bulk skin possessing native optical properties, and a compressed skin region underneath the pin. This compressed region was defined from the mechanical finite element simulation output as the region comprised of all elements with minimum principal logarithmic strain of at least −50%, corresponding to a region with significant tissue compression resulting in modified optical properties. Such a compressed region was selected because, to our knowledge, the spatial distribution of water content and resulting distribution of optical properties during TOCD application is not currently well understood. The shape of this 50% compressive strain region as well as the deformed shape of the skin sample were traced and subsequently sketched in a new composite medium for nominal tissue strains of 0, 25, and 50%. Each model was assigned a mesh of tetrahedral (C3D4) elements with 0.2 mm approximate edge size. The meshes for models of 0, 25, and 50% nominal strain contained 574,511, 523,469, and 447,071 elements, respectively. The lower strain models have higher element counts because a larger air region is required to reach the top of the pin

from the skin surface. Also, the sides of the skin sample were assumed to not deform since this edge deformation results in low strain and would not be observed in larger samples. The optical properties of the environment outside the mesh boundary surfaces, chosen to be air, were specified in order to define transmission at these medium boundaries.

While the mechanical simulations used an 8 mm × 8 mm × 2.5 mm skin sample, using this size skin sample in Monte Carlo simulations would result in significant (>5% of all generated photons) photon loss through the sides of the simulation space, adversely affecting light transmission calculations through the bottom of the glass slide. The simulated skin sample and glass slide were expanded to be 12.5 mm on a side instead of 8 mm. This change in skin sample size does not affect the compressed tissue geometry since the traced deformed skin surface region has a radius of no more than approximately 6 mm. The dimension 12.5 mm was selected to match the size of the optical power collector used experimentally.[17]

The light source was defined as a series of collimated light beams impinging on each triangular element surface on the top surface of the pin. The amount of photons delivered in each beam was weighted such that each triangular element surface had the same fluence, or number of photons per area. A total of 10^8 photons was used in each simulation. Baseline optical properties for each region were defined as in Table 2. These properties were selected assuming that light being transmitted through the medium had a wavelength of 633 nm.

TIM-OS calculates photon fluence, Φ, as

$$\Phi = \frac{w_a}{V\mu_a}, \tag{2}$$

where Φ is the photon fluence, w_a is the sum of the absorbed photon weights for a region, V is the volume of the region, and μ_a is the absorption coefficient. Equation (2) shows that TIM-OS will have difficulty quantifying photon fluence for a zero absorption region. To solve this problem, we assigned extremely low absorption parameters for air and glass regions relative to values of the absorption coefficient of skin as shown in Table 2.

We first simulated light transmission through the glass pin in direct contact with the glass slide without a skin sample present. This transmission value will serve as a baseline transmission, the maximum possible attainable transmission during subsequent pin compression simulations, mimicking baseline definition used experimentally.[17] We then investigated the effects of nominal tissue strain on tissue light transmission by performing Monte Carlo simulations for meshed media constructed from 0, 25, and 50% strain finite element outputs. Light transmission was defined as the number of photons exiting through the bottom surface of the glass slide divided by the number of photons input to the model. This measure of light transmission is relevant to experiments where an optical power wand could be inserted under the slide as described previously.[17] We also chose to investigate the effects of changing the absorption coefficient, μ_a, scattering coefficient, μ_s, and refractive index, n, of the compressed skin region. We chose to ignore changes in the anisotropy factor, g, due to tissue strain, leaving g constant for all skin regions in each simulation. The modified optical properties used for each simulation are shown in Table 3. In simulations 4 through 9, one of the three varying optical properties was changed to a moderately altered value or a highly altered value, holding the other parameters

Table 2. Baseline optical properties used in simulating the effects of geometry change on light transmission.

	μ_a [mm^{-1}]	μ_s [mm^{-1}]	n [–]	g [–]
Air	0.001	0.001	1.003	1.000
Glass	0.001	0.001	1.458*	1.000
Skin	0.089†	28.9†	1.38‡	0.926†

*Value for SiO_2 glass at 632.8 nm.[22]
†Value for porcine dermis at 632.8 nm.[23]
‡Value for porcine skin at 850 nm.[15]

Table 3. Values for parameter study of optical properties in compressed skin region at 50% nominal tissue strain. Gray regions highlight changes in optical properties from baseline values.

Simulation	Nominal strain [%]	μ_a [mm^{-1}]	μ_s [mm^{-1}]	n [–]
1	0	0.0890	28.9	1.38
2	25	0.0890	28.9	1.38
3	50	0.0890	28.9	1.38
4	50	0.0712	28.9	1.38
5	50	0.0534	28.9	1.38
6	50	0.0890	23.12	1.38
7	50	0.0890	17.34	1.38
8	50	0.0890	28.9	1.449
9	50	0.0890	28.9	1.518
10	50	0.0712	23.12	1.449
11	50	0.0534	17.34	1.518

constant. The absorption and scattering coefficients were each reduced to either 80% or 60% of the original value, while refractive index was increased to either 105% or 110% of its original value. The refractive index was chosen within these ranges because the refractive index of optically cleared skin cannot exceed that of the protein constituents, approximately 1.53 for dry collagen.[24] For simulations 10 and 11, all three optical properties were changed to either the moderately or highly altered value. This multivariate change in optical properties is more realistic as water transport will affect all three of these parameters simultaneously. All optical Monte Carlo simulations were performed on a work station with two quad-core Xeons (L5520). Each simulation took approximately 11 minutes for 10^8 photons.

3. Results and Discussion

Results from the mechanical finite element simulation for 50% nominal tissue strain are shown in Fig. 5. These plots verify that the highest logarithmic or true strain occurs immediately under the pin and then drops off laterally. From this strain profile, the region of elements with logarithmic compressive strain of at least 50% was subsequently incorporated into each contiguous meshed medium for Monte Carlo simulation. For all simulations, the amount of photons exiting from the side surfaces of the mesh was less than 3.5% of the 10^8 photons generated during simulation, ensuring that light transmission through the bottom mesh surface was not affected by mesh boundary positioning. The internal element fluence distribution resulting from select Monte Carlo simulations is plotted in Fig. 6 for simulations 1, 3, 10, and 11. It is evident that pin compression alone has a significant focusing effect and increase in fluence at the bottom surface of the glass slide. The additional effect of changing skin optical properties also increases fluence, but this effect is difficult to quantify by inspecting Fig. 6. The light transmission through the bottom surface of the slide, T, was calculated for each simulation as presented in Table 4. Changes in the scattering coefficient were found to have the largest effect on transmission (28.9%), followed by index of refraction (19.9%) and finally absorption coefficient (6.5%). These findings also suggest that compression-dependent changes in tissue geometry alone have a significant optical clearing effect, increasing transmission from 10% to 41%. The transmission calculations also show that changing the optical properties by significant yet realistic amounts provides an additional increase in transmission from 41% to 69%. More modest changes in optical properties resulted in transmission increasing from 41% to 57%, indicating that both compression-driven geometry change and changing optical properties significantly increase transmission, with geometry contributing approximately 52–66% of the total increase in light transmission.

While this preliminary model predicts that the total optical clearing effect on transmission may be anywhere from a four-fold to approximately a six-fold increase, this result should be interpreted with caution as light transmission experiments have demonstrated a three-fold to four-fold increase in

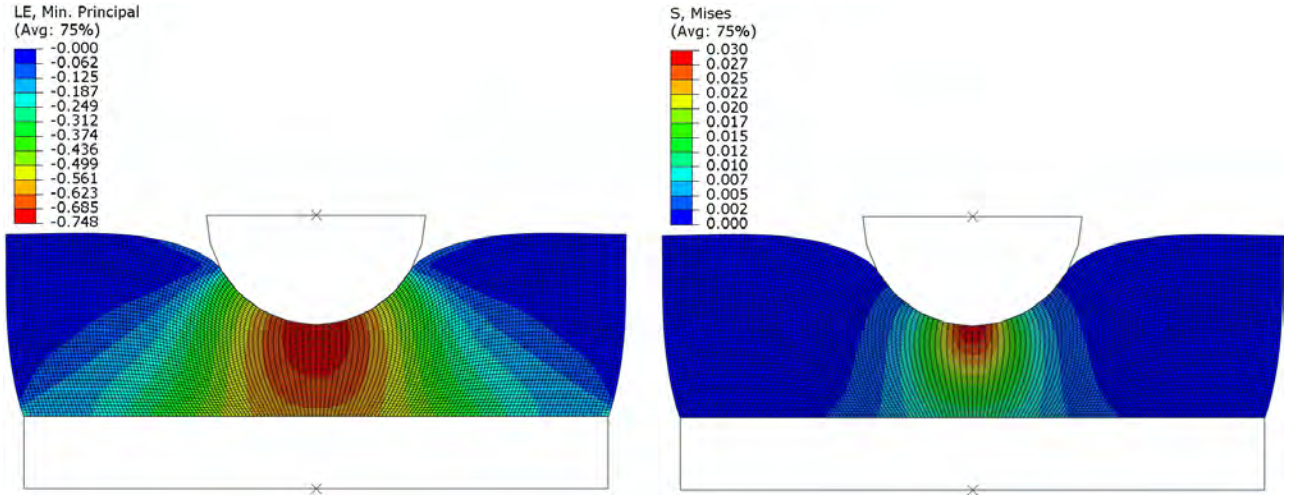

Fig. 5. Stress and strain distributions resulting from mechanical simulation. Stress reported in MPa.

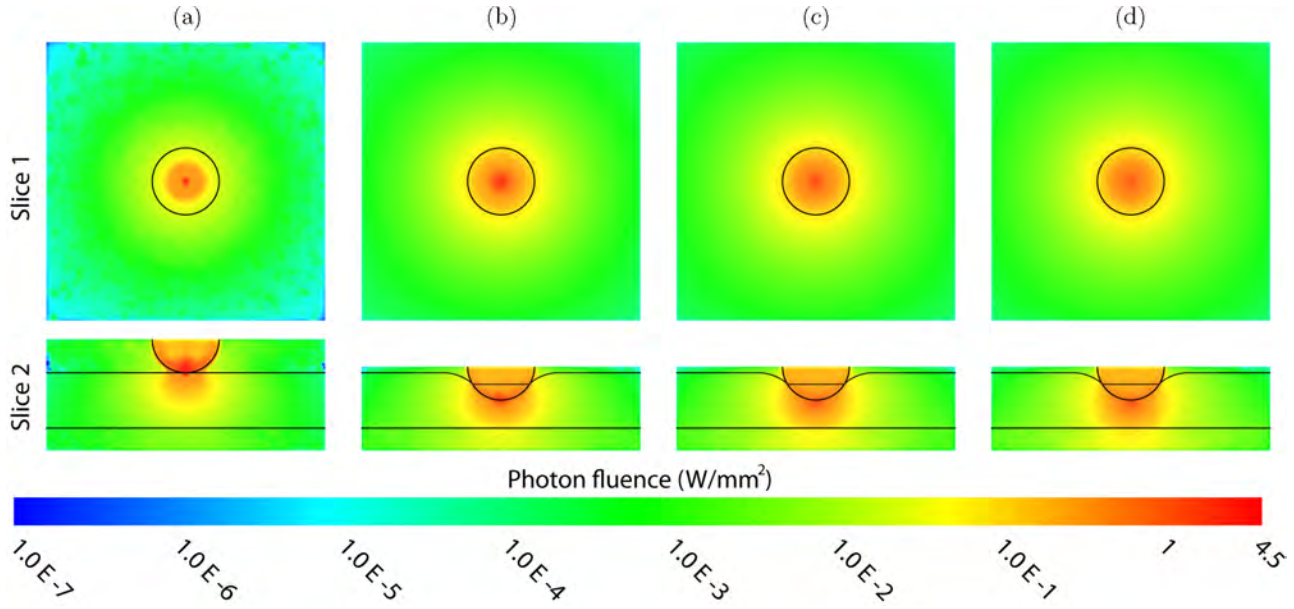

Fig. 6. Internal element fluence distributions for optical Monte Carlo simulations (a) 1, (b) 3, (c) 10, and (d) 11. Slice 1 is a horizontal slice taken at the height of the tip of the pin, while Slice 2 is taken through the center of the pin.

Table 4. Transmission results from each Monte Carlo simulation. Simulation 0 is simulation of the pin in direct contact with the glass slide without a skin sample in between.

Simulation	T [%]	T relative to glass only case [%]	T relative to 50% strain case [%]
0	41.48	100.0	—
1	4.22	10.17	—
2	8.76	21.12	—
3	17.15	41.35	100.0
4	18.06	43.54	105.3
5	18.27	44.05	106.5
6	19.00	45.81	110.8
7	22.11	53.30	128.9
8	20.11	48.48	117.3
9	20.57	49.69	119.9
10	23.68	57.09	138.1
11	28.86	69.43	167.9

light transmission during local pin compression at 50% and 75% nominal strain, respectively.[17] This difference between model predicted and observed transmission values is largely due to the simulated baseline transmission through skin being lower than the baseline transmission measured experimentally (∼20%).[17] This is likely the result of simulating a thicker skin sample (2.5 mm) than those used in transmission experiments (∼1.5 mm) because a thicker medium will scatter and absorb more light than a thinner medium, lowering transmission.[17] Future work could include studying the effects of varying tissue thickness and other geometric considerations.

Another limitation of this study is the simplified mechanical skin model used in finite element simulation, which only used pin compression data. Hyperelastic material law identification by regression is capable of accepting multiple input stress/strain datasets in different deformation modes to fit the material law. By only using localized pin compression stress/strain information, the hyperelastic material model was determined without considerations of skin's behavior in other modes of deformation, including uniaxial tension, shear, biaxial tension, and uniaxial (not localized) compression. The elements in the finite element model undergo combinations of these modes of deformation, and so a more complete mechanical dataset would result in a hyperelastic material model that would lead to more accurate modeling predictions of spatial tissue strain distributions.

We have also not yet included a finite element model to describe water transport due to strain fields in the tissue. Rather, we have assumed a threshold strain value for which optical properties were disjointedly modified. The actual change in optical properties will be a continuous spatiotemporal function of local tissue water content, and so a model of tissue water transport during TOCD application is required in order to correctly predict

water transport and resulting changes in optical properties. A more comprehensive model of tissue deformation, modified tissue water content and optical property distributions would provide a more accurate description of light distribution in mechanical tissue optical clearing.

4. Conclusions

Through combined mechanical finite element modeling and optical Monte Carlo simulation, we have demonstrated the ability to model and investigate the application of TOCDs to skin. The results indicate that changes in both tissue geometry due to compression and changes in optical properties due to tissue strain can potentially contribute to mechanical optical clearing. There are, however, several crucial additions to the model to be made in order to allow comparison to experimental data, including robust mechanical modeling, correlation between mechanical response and tissue water transport, and correlation between tissue water content and optical properties. By investigating these model domains and collecting data for tuning the model, a multi-domain model could be used to accurately predict changes in light transport during application of TOCDs. This would provide a tool for optimizing the design of such devices for diagnostic and therapeutic applications.

Acknowledgments

This research was funded in part by NIH BRP grant #1R01HL098912-01 and by a fellowship for William C. Vogt provided by the Institute for Critical Technology and Applied Science (ICTAS) Doctoral Scholars Program at Virginia Tech.

References

1. V. V. Tuchin, *Optical Clearing of Tissues and Blood*, SPIE Press, Bellingham, WA (2006).
2. J. Yoon, T. Son, E. H. Choi, B. Choi, J. S. Nelson, B. Jung, "Enhancement of optical skin clearing efficacy using a microneedle roller," *J. Biomed. Opt.* **13**(2), 021103 (2008).
3. G. Vargas, J. K. Barton, A. J. Welch, "Use of hyperosmotic chemical agent to improve the laser treatment of cutaneous vascular lesions," *J. Biomed. Opt.* **13**(2), 021114 (2008).
4. X. Xu, Q. Zhu, C. Sun, "Assessment of the effects of ultrasound-mediated alcohols on skin optical clearing," *J. Biomed. Opt.* **14**(3), 034042 (2009).
5. M. Zimmerley, R. A. McClure, B. Choi, E. O. Potma, "Following dimethyl sulfoxide skin optical clearing dynamics with quantitative nonlinear multimodal microscopy," *Appl. Opt.* **48**(10), D79–D87 (2009).
6. J. Hirshburg, B. Choi, J. S. Nelson, A. T. Yeh, "Correlation between collagen solubility and skin optical clearing using sugars," *Lasers Surg. Med.* **39**(2), 140–144 (2007).
7. B. Choi, L. Tsu, E. Chen, T. S. Ishak, S. M. Iskandar, S. Chess, J. S. Nelson, "Determination of chemical agent optical clearing potential using *in vitro* human skin," *Lasers Surg. Med.* **36**(2), 72–75 (2005).
8. X. Wen, Z. Z. Mao, Z. Z. Han, V. V. Tuchin, D. Zhu, "*In vivo* skin optical clearing by glycerol solutions: Mechanism," *J. Biophotonics* **3**(1–2), 44–52 (2010).
9. E. A. Genina, A. N. Bashkatov, A. A. Korobko, E. A. Zubkova, V. V. Tuchin, I. Yaroslavsky, G. B. Altshuler, "Optical clearing of human skin: Comparative study of permeability and dehydration of intact and photothermally perforated skin," *J. Biomed. Opt.* **13**(2), 021102 (2008).
10. C. H. Liu, Z. W. Zhi, V. V. Tuchin, Q. M. Luo, D. Zhu, "Enhancement of skin optical clearing efficacy using photo-irradiation," *Lasers Surg. Med.* **42**(2), 132–140 (2010).
11. C. G. Rylander, O. F. Stumpp, T. E. Milner, N. J. Kemp, J. M. Mendenhall, K. R. Diller, A. J. Welch, "Dehydration mechanism of optical clearing in tissue," *J. Biomed. Opt.* **11**(4), 041117 (2006).
12. G. Vargas, E. K. Chan, J. K. Barton, C. G. Rylander, A. J. Welch, "Use of an agent to reduce scattering in skin," *Lasers Surg. Med.* **24**(2), 133–141 (1999).
13. A. T. Yeh, B. Choi, J. S. Nelson, B. J. Tromberg, "Reversible dissociation of collagen in tissues," *J. Invest. Dermatol.* **121**(6), 1332–1335 (2003).
14. R. K. Wank, X. Xu, "Concurrent enhancement of imaging depth and contrast for optical coherence tomography by hyperosmotic agents," *J. Opt. Soc. Am. B* **18**(7), 948–953 (2001).
15. C. Drew, T. E. Milner, C. G. Rylander, "Mechanical tissue optical clearing devices: Evaluation of enhanced light penetration in skin using optical coherence tomography," *J. Biomed. Opt.* **14**(6), 064019 (2009).
16. C. G. Rylander, T. E. Milner, S. A. Baranov, J. S. Nelson, "Mechanical tissue optical clearing devices: Enhancement of light penetration in *ex vivo* porcine skin and adipose tissue," *Lasers Surg. Med.* **40**(10), 688–694 (2008).
17. A. Izquierdo-Roman, C. G. Rylander, "Measurement of increased light transmission and strain as a function of mechanical compression in *ex vivo* porcine skin," *Lasers Surg. Med.* **42**(S22), 9 (2010).

18. I. W. Busbridge, *The Mathematics of Radiative Transfer*, Cambridge University Press [Eng.], p. 143 (1960).
19. A. D. Kim, "Transport theory for light propagation in biological tissue," *J. Opt. Soc. Am. A Opt. Image Sci. Vis.* **21**(5), 820–827 (2004).
20. S. Arridge, "Optical tomography in medical imaging," *Inverse Prob.* **15**, R41–R93 (1999).
21. H. Shen, G. Wang, "A tetrahedron-based inhomogeneous Monte Carlo optical simulator," *Phys. Med. Biol.* **55**(4), 947–962 (2010).
22. *CRC Handbook of Chemistry and Physics*, Ed. D. R. Lide, CRC Press (2010).
23. A. J. Welch, M. J. C. van Gemert, *Optical-Thermal Response of Laser-Irradiated Tissue*, Ed. H. Kogelnik, Plenum Press, New York (1995).
24. X. Wang, T. E. Milner, M. C. Chang, J. S. Nelson, "Group refractive index measurement of dry and hydrated type I collagen films using optical low-coherence reflectometry," *J. Biomed. Opt.* **1**(2), 212–216 (1996).